North Atlantic storm driving of extreme wave heights in the North Sea

AGU PUBLICATIONS

JGR

Journal of Geophysical Research: Oceans

RESEARCH ARTICLE
10.1002/2016JC012501

North Atlantic storm driving of extreme wave heights in the North Sea

R. J. Bell[1], S. L. Gray[2], and O. P. Jones[3]

[1]Department of Meteorology and Physical Oceanography, Rosenstiel School of Marine and Atmospheric Science, University of Miami, Miami, Florida, USA, [2]Department of Meteorology, University of Reading, Reading, Berkshire, UK, [3]BP, Sunbury-on-Thames, Middlesex, UK

Key Points:
- Extreme wave events can be clustered in northerly and southerly-wind events
- Winds in the cold conveyor belt of extratropical cyclones on average cause the largest wave heights
- Ensemble sensitivity analysis shows wave height is sensitive to sea-level pressure two days prior

Correspondence to:
R. J. Bell,
rbell@rsmas.miami.edu

Citation:
Bell, R. J., S. L. Gray, and O. P. Jones (2017), North Atlantic storm driving of extreme wave heights in the North Sea, *J. Geophys. Res. Oceans*, *122*, doi:10.1002/2016JC012501.

Received 25 OCT 2016
Accepted 27 MAR 2017
Accepted article online 4 APR 2017

Abstract The relationship between storms and extreme ocean waves in the North Sea is assessed using a long-period wave data set and storms identified in the Interim ECMWF Re-Analysis (ERA-Interim). An ensemble sensitivity analysis is used to provide information on the spatial and temporal forcing from mean sea-level pressure and surface wind associated with extreme ocean wave height responses. Extreme ocean waves in the central North Sea arise due to intense extratropical cyclone winds from either the cold conveyor belt (northerly-wind events) or the warm conveyor belt (southerly-wind events). The largest wave heights are associated with northerly-wind events which tend to have stronger wind speeds and occur as the cold conveyor belt wraps rearward round the cyclone to the cold side of the warm front. The northerly-wind events provide a larger fetch to the central North Sea to aid wave growth. Southerly-wind events are associated with the warm conveyor belts of intense extratropical cyclones that develop in the left upper tropospheric jet exit region. Ensemble sensitivity analysis can provide early warning of extreme wave events by demonstrating a relationship between wave height and high pressure to the west of the British Isles for northerly-wind events 48 h prior. Southerly-wind extreme events demonstrate sensitivity to low pressure to the west of the British Isles 36 h prior.

Plain Language Summary This study investigates how large-scale storms, known as extratropical cyclones, are related to extreme wave events in the North Sea. The North Sea houses oil and gas platforms as well as provides passage to cruise ships, thus, extreme wave events can impact the safety of ongoing operations in these industries. For this study, we examined 20 years of data to determine what storms led to extreme wave events and what characteristics those storms, or the environment that they are in, have in common. We found that in the two days prior to a storm which results in an extreme wave event, the strengthening of a high pressure system to the west of the British Isles was key. These new findings can improve warnings of extreme wave events in the North Sea and therefore enhance safety for industry operations.

1. Introduction

The North Sea is home to a large number of permanently manned fixed and floating oil production platforms, manned mobile drilling units and installation vessels. The intensity of storms in the region and the risks involved in demanning platforms during severe weather emphasize the importance of high-quality weather forecasting. An improved understanding of synoptic-scale weather conditions that lead to extreme wave heights in the North Sea could improve the predictability of severe events and provides the motivation for this paper.

One common measurement of ocean wave height is significant wave height (H_s). This is approximately equal to the mean of the highest one third of the waves in a sea-state (description of sea surface waves over 10–30 min). H_s is calculated based on the variance density spectrum of surface elevation. The value of H_s represents the interplay of energy input from the wind (either locally or remote) and energy lost through processes such as dissipation. The large-scale wave energy input from the wind is determined by the fetch, the speed of the wind, and the duration; these are all controlled by the state of the atmosphere. A first-order understanding of how H_s responds to these factors can be deduced from a Nomogram (e.g., a

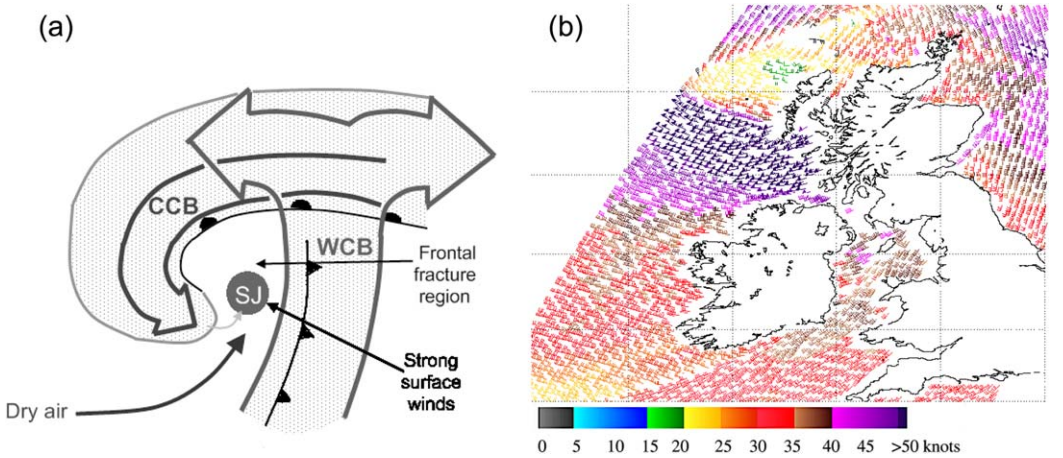

Figure 1. (a) Conceptual conveyor belt air flow model for extratropical cyclones. Fronts are shown using conventional notation. Reproduced from *Baker et al.* [2014] with permission ([copyright] 2013 Royal Meteorological Society). (b) NOAA wind vectors (10 m neutral stability winds) from the Advanced Scatterometer (ASCAT METOP-A) for extratropical cyclone Friedhelm on 8 December 2011 (descending pass). Image courtesy of NOAA\NESDIS Center for Satellite Applications and Research.

Sverdrup-Munk-Bretschneider Nomogram). Another factor that is important for wave growth is the synoptic-scale weather evolution. For example, *Ponce de León and Guedes Soares* [2014] found the probability of occurrence of extreme waves (associated with the strong winds) is greatest in the bent-back front of extratropical cyclones. In addition, extreme waves can occur in situations of a "trapped-fetch" [*Reistad et al.*, 2005; *Kudryavtsev et al.*, 2015], where a weather system is moving at the same speed as the group velocity of the waves and therefore providing the waves with continual forcing for growth.

The North Atlantic Ocean is home to the largest extreme waves in the world [*Breivik et al.*, 2014] due to the behavior of extratropical cyclones. Both the largest H_s [*Hanafin et al.*, 2012] and the lowest extratropical cyclone mean sea-level pressure (MSLP) [*Odell et al.*, 2013] have occurred in the North Atlantic making this location the most hazardous to the offshore industry [*Cardone et al.*, 2015]. The primary North Atlantic storm track, defined as the band of climatological maximum track density of extratropical cyclones, extends from the strongly baroclinic zone off Cape Hatteras in the west Atlantic across Iceland; a secondary track (weaker density) extends from the mid North Atlantic over northern Europe [e.g., see *Hoskins and Hodges*, 2002, Figure 14 and *Dacre and Gray*, 2009, Figure 5]. Hence, cyclones affecting North Sea oil and gas platforms are typically mature cyclones. The clustering of extratropical cyclones in recent years caused wave damage along the coast in Western Europe [*Pinto et al.*, 2014]. Storm clustering tends to increase H_s by providing energy to a sea-state that already contains energy associated with a previous storm. Mesoscale features within an extratropical cyclone are also important for H_s [*Cavaleri et al.*, 2016].

The air flows in extratropical cyclones can be represented by the conveyor belt conceptual model e.g., *Browning and Roberts* [1994]. Figure 1a shows the three characteristic air flows: the warm conveyor belt (WCB) extending along the main cold front and rising over the warm front where it splits into lower cyclonic and upper anticyclonic turning branches; the cold conveyor belt (CCB) wrapping rearward round the cyclone to the north of the warm front; and the dry intrusion (dry air) descending from the upper troposphere toward the top of the atmospheric boundary layer. Also shown is the location of strong near surface winds attributable to a sting jet (SJ), a mesoscale jet of strong winds, and especially strong gusts, which occurs behind the cold front in some cyclones over a period of several hours. *Martínez-Alvarado et al.* [2012] found that up to a third of a set of 100 winter North Atlantic cyclones satisfied the conditions for sting jets. Sustained strong surface winds occur associated with the WCB and, in mature storms, with the end of the CCB [*Hewson and Neu*, 2015]. The cold front wraps around the low pressure center as the system matures, and the wind direction in the CCB aligns with that of the environmental westerly flow and so can be associated with extreme localized winds [*Browning*, 2005].

These strong wind regions are illustrated for an example cyclone, windstorm Friedhelm (2011), using ocean surface winds derived from advanced scatterometer (ASCAT) observations (Figure 1b). The center of the cyclone is to the northwest of Scotland at this time (the empty data region at about 59°N, 7°W). The winds

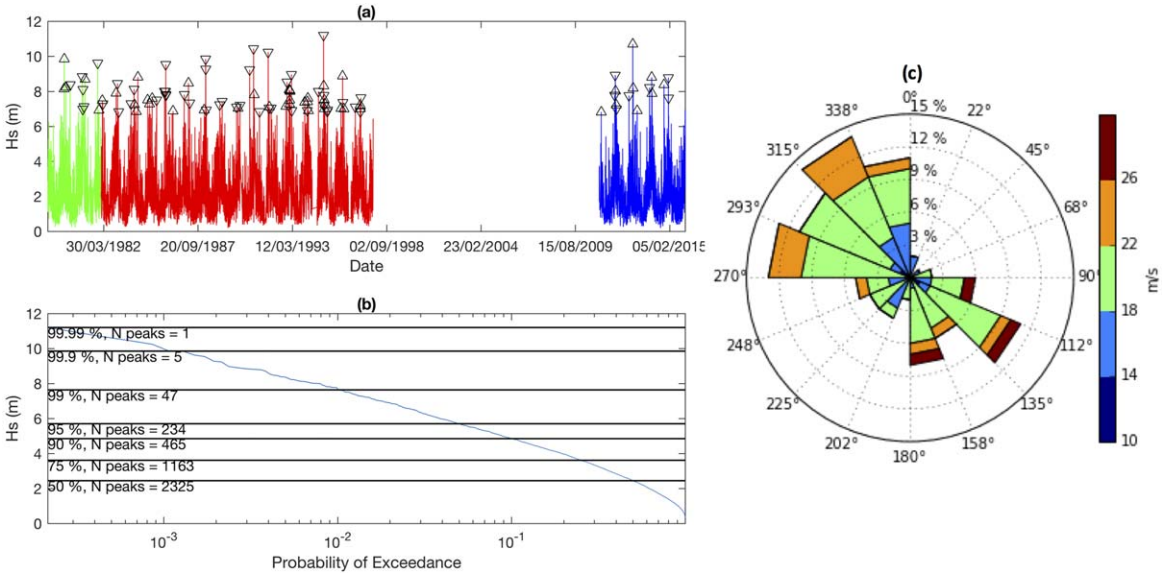

Figure 2. (a) Time series of measured H_s described in Table 1 (the three different colors are used to distinguish the three data periods). The 100 most extreme events are indicated by black triangles (downward-pointing triangles for northerly-wind events and upward-pointing triangles for southerly-wind events; see plot c). (b) Probability of exceedance of H_s peaks. The horizontal lines are labeled as percentiles and the number of events. The total number of peaks is 4650. (c) Wind rose of the 100 most extreme H_s events. The angle shows the direction from north that the wind is coming from and the magnitude is the number of events.

exceeding 50 knots to the west of Scotland are associated with the CCB; *Martínez-Alvarado et al.* [2014] also diagnose the presence of a sting jet in this region at this time. The cold front runs along the southern coast of Ireland (e.g., see 1200 UTC Met Office surface analysis in Figure 2b of *Martínez-Alvarado et al.* [2014]) and is associated with a sharp line of wind direction change in Figure 1b. The bands of locally stronger winds to the southeast of Ireland and over the North Sea are associated with the WCB, inferred from their position relative to the cold front and comparison with the model forecast low-level winds shown in Figure 3b of *Martínez-Alvarado et al.* [2014] (which have the advantage of being defined over land as well as the ocean).

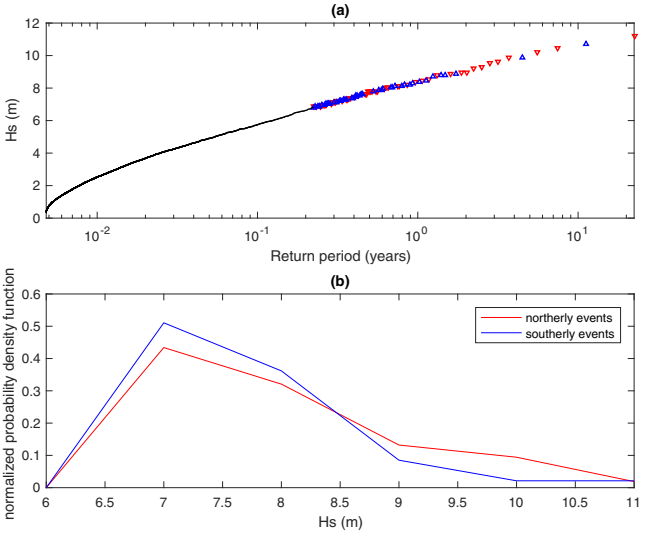

Figure 3. Measured H_s at the Forties platform. (a) Return period. The 100 most extreme events are indicated by triangles (red downward-pointing triangles for northerly-wind events and blue upward-pointing triangles for southerly-wind events). (b) Normalized probability density function of H_s peaks for northerly-wind events (red) and southerly-wind events (blue).

The purpose of this study is to determine the evolution of synoptic conditions climatologically associated with extreme H_s values in the North Sea. There have only been a few previous climatological studies of the relationship between atmospheric conditions and H_s values: *Ortiz-Royero et al.* [2013] associated extreme wave events in the Caribbean Sea with cold frontal events; *Pingree-Shippee et al.* [2016] investigated a few case studies of storms and extremes wave heights in the Bering and Chukchi Sea and found stationary storms produce the largest, steepest waves. Previous studies for the North Atlantic have only looked at one event in detail [*Hanafin et al.*, 2012; *Gibson et al.*, 2014; *Cavaleri et al.*, 2016]. *Camus et al.* [2014] looked at the relationship between MSLP and sea-level pressure gradient relating to present-day and future wave climate. The 100 weather

patterns *Camus et al.* [2014] identify represent modes of atmospheric variability such as the North Atlantic Oscillation and the East Atlantic Pattern. In our study, individual storms are treated as ensemble members and the sensitivity of H_s at a particular location to the MSLP and wind speed is investigated.

The paper is structured as follows. The data sets and the ensemble sensitivity analysis method are described in section 2. The atmospheric synoptic-scale evolutions associated with extreme wave height events are provided in section 3. Finally, the discussion and conclusions are given in section 4.

2. Data and Methodologies

2.1. Measured Wave Data

Measured wave data are used from the Forties platform in the central North Sea (57.8°N, 0.9°E). The data set includes several multiyear periods of measurements of the sea surface elevation since 1974. Most wave measurement data sets are only available from the 2000s or in some cases the 1990s. Hence, this data set covers a relatively long-time period, including a period from when few ocean wave measurements are available. It encompasses many extreme wave events and provides wave data for historic storms [*Feser et al.*, 2015]. Only one location in the central North Sea is used in this study to enable a detailed analysis of relevant storms and to build up climatologies. The measured wave data sets are summarized in Table 1 and described further below.

The first data set (1974–1982) contains measurements from a Datawell Waverider Buoy and Baylor Wavestaff which were recorded on analogue magnetic tapes. The analogue records were subsequently digitized at two Hz at 3 hourly intervals. The duration of each record was 1024 s and H_s was derived as four times the root-mean-square of surface elevation ($H4_{rms}$). The second data set (1982–1997) used the same instruments, but provides H_s at 1 hourly intervals. The third data set (2011–2015) provides H_s given at 6 hourly intervals computed as four times the square root of the zeroth-order moment of the wave spectrum (H_{m0}) from a SAAB REX WaveRadar. Temporal averaging is required to reduce uncertainties in the estimate of the significant wave height [*Gemmrich et al.*, 2016]. The Forties wave data set thus provides approximately 28 years of measurements, as shown in Figure 2a.

The wave data sets are used from 1979 onward, which is when detailed information is available on the state of the atmosphere (see section 2.3). For the first two data sets, H_s is calculated as a 3 h running root-mean-square average. The method to calculate H_s in the third data set is provided in *Bidlot et al.* [2002] and represents a 3 hourly average. The H_s values at 0000, 0600, 1200, and 1800 UTC are retained for use with the 6 hourly atmospheric reanalysis data.

2.2. Extreme Wave Events

Extreme H_s events are obtained from the wave data set using a peak-over-threshold methodology [*Leadbetter*, 1991]. Each maximum of H_s is retained and, if multiple large values exist for neighboring time steps, only the largest H_s is selected. The next event is selected using an interval between maxima of at least one day. This ensures that multiple extreme H_s events are not sampled within the same storm. Figure 2b shows the number of events associated with different H_s threshold levels. For example, only one event has a 3 hourly average H_s greater than 11 m and only two events are greater than the 10 year return period value of H_s (10.6 m; Figure 3a). We use 100 events in total which is equal to the 97.8th percentile of peak events. The 100 events provide a large enough sample size to create climatologies of extreme H_s events yet ensure we remain focused on the largest wave heights. The events are split into northerly and southerly-wind events at the time of the extreme H_s event. Two dominant wind direction clusters can be seen for these cases: winds from the north-west and south-east (Figure 2c). The largest wave events are associated with northerly-wind as shown in Figure 3a despite there being a prevalence of very strong winds from the southerly direction (shown by the higher wind speeds in the wind rose (Figure 2c). There is almost an even split of the 100 largest wave events from the north (53

Table 1. Measured Wave Data Sets Available From the Forties Platform (0.9°E, 57.75°N)

Period	Frequency	Instrument
7/12/1974 to 1/27/1982	3 hourly	Datawell Waverider Buoy and Baylor Wavestaff
2/5/1982 to 11/18/1997	hourly	Datawell Waverider Buoy and Baylor Wavestaff
1/1/2011 to 12/31/2015	6 hourly	SAAB REX WaveRadar

events) and the south (47 events). A normalized probability density function, given in Figure 3b, shows the majority of the southerly-wind associated H_s events are between 6 and 9 m with an asymptotic tail shape, reflecting a fetch limit.

2.3. ERA-Interim

The European Centre for Medium-Range Weather Forecasts (ECMWF) Interim Re-Analysis (ERA-Interim) is used to provide information on the synoptic-scale atmospheric evolution. This reanalysis is based on the predictions of a weather forecast model constrained by assimilation of data [*Dee et al*., 2011]. The horizontal resolution of ERA-Interim is 80 km (T255). Northern Hemisphere winter extratropical cyclones in the ERA-Interim reanalysis have been shown to agree well with those in three other recent high-resolution reanalyses in terms of the spatial distribution, number and intensity of storms, and the number of matched storms [*Hodges et al*., 2011]. The conveyor belt structure of cyclones shown in Figure 1a is also represented well by ERA-Interim. *Hodges et al*. [2011] show that composites low-level wind and MSLP fields, constructed using the 100 most intense cyclones in ERA-Interim, are very consistent with composites generated using matched storms in the three other reanalyses.

2.4. Extratropical Cyclone Tracking Algorithm

The extratropical cyclone tracking scheme developed in *Hodges* [1994] and *Hodges et al*. [2011] is used in this study. Cyclones are identified as maxima in the 850 hPa relative vorticity in the 6 hourly ERA-Interim data. The vorticity fields are truncated to T42 resolution prior to use to emphasize the synoptic scales. The tracks are filtered to retain storms that last at least 2 days and travel farther than 1000 km. The tracks of cyclones associated with the identified extreme wave events are extracted as follows. First, all tracks that include a cyclone within a specified domain close to the Forties platform at the time of the extreme event are extracted from the track database. Second, the locations of the cyclones at the time of the events are plotted on maps of MSLP and wind to determine which, if any, of the tracked cyclones match the cyclone subjectively judged to be directly associated with the strong winds at the Forties platform. Finally, the track files are manually edited to retain only tracks of those cyclones associated with the extreme wave events (a maximum of one track for each event). In most cases, the cyclone associated with the extreme wave event was easily identifiable and present in the track database. In a small number of cases, the associated cyclone was not present in the tracks database and so a track was not identified for that event (see caption of Figure 10 for details); however, this small number of missing tracks does not affect the conclusions drawn.

2.5. Ensemble Sensitivity Analysis

The environmental conditions (MSLP and 10 m wind speed (U_{10}) structures) preferentially associated with extreme values of H_s are diagnosed using the ensemble sensitivity technique described by *Garcies and Homar* [2009] and *Dacre and Gray* [2013]. These preferential conditions are diagnosed at 6 hourly intervals from 2 days before to 12 h after the time of the extreme H_s. Following previously published papers, the extreme H_s values are described as *sensitive* to the environmental conditions; however, mathematically the calculation merely yields an association and results must be interpreted considering dynamical plausibility. A set of extreme H_s events is termed a "response function" (J). Two response functions are considered: subsets of top 100 events with northerly and southerly flow at Forties at the time of the event (53 and 47 events, respectively; see triangles in Figure 2a. For each response function, MSLP and U_{10} fields are extracted from ERA-Interim for each time required. Maps of the sensitivity of the response function to each of these fields at each specified time (e.g., 2 days prior to events) are produced following the method described in *Dacre and Gray* [2013] and summarized here. These sensitivity maps can be interpreted as showing the change in H_s associated with a one standard deviation increase (decrease) in the chosen field at the chosen time relative to events. A linear regression is calculated at each spatial grid point, (i, j), between the values of the response function and difference of the chosen field from the mean value (over the events), x, yielding a regression coefficient:

$$R_{ij} = \left(\frac{\partial J}{\partial x}\right)_{ij}.$$

A correction factor is then applied to filter out weak correlations:

$$C_{ij} = \begin{cases} 1 & \text{if } r_{ij}^2 \geq c^2 \\ \dfrac{r_{ij}^2}{c^2} & \text{if } r_{ij}^2 < c^2, \end{cases}$$

where r_{ij} is the correlation coefficient and c is the minimum correlation coefficient for which the raw sensitivities remain unaltered. This coefficient is set to 0.05 here following *Dacre and Gray* [2013]. This leaves the sensitivities to MSLP (U_{10}) at 81 (587) and 502 (687) of the 4700 grid points uncorrected at the time of the southerly and northerly-wind events, respectively (these values are strongly time-dependent). The sensitivity, S_{ij}, is then given by multiplying the regression coefficient by the correction factor and the standard deviation of the field at that grid point yielding

$$S_{ij} = R_{ij} C_{ij} \sigma_{ij},$$

where the units of S_{ij} are thus the same as those of J (i.e., m).

3. Results

3.1. Case Studies of Extreme Wave Events

The largest H_s event within the data set occurred at the Forties platform in the central North Sea on New Year's Day 1995 and was associated with northerly-winds occurring in the CCB of an extratropical cyclone. This storm is infamous for producing the Draupner wave (the first instrument-recorded freak wave at the Draupner platform) which is discussed fully in *Cavaleri et al*. [2016]. Figures 4a–4i shows the atmospheric synoptic evolution of this event from 48 h prior to the event (T-48) to 12 h after it (T+12); time series of 10 m wind speed and direction determined from the ERA-I data and measured H_s at the Forties platform are shown in Figure 4j). Two days before the extreme event, there was a low pressure system situated over the location of the Forties platform. At this time, the strongest winds were northerly to the west of the British Isles, occurring in the CCB. The center of the low moved slowly to the south east over the next 2 days. A high pressure center to the west also strengthened during this time, resulting in a strong pressure gradient across the North Sea and therefore strong geostrophic winds. The most intense winds at the time of the largest wave height (T0, Figure 4g) are associated with winds wrapping around the low pressure system leading to the superposition of storm-relative and background westerly winds. Sting jets can also occur in this region of the cyclone (see Figure 1a).

Figure 5 shows the synoptic evolution and measured H_s at the Forties platform yielding the largest H_s associated with southerly-wind of an extratropical cyclone. On 15 December 2012, embedded within a stationary larger-scale low pressure system, a cyclone to the south-west of the platform caused large wave heights at the Forties platform with strong south-easterly winds. *Gibson et al*. [2014] found 19 freak waves occurred during this storm across the North Sea. Compared to the northerly-wind case study, the increase in H_s was rapid: an increase from about 1 to 10.7 m in 24 h (Figure 5j). At T-18 (Figure 5d) a secondary cyclone formed to the east of the already formed low pressure center and moved eastward. At T0 (Figure 5g), the winds are strongest in the north-east quadrant of the storm along a fetch that stretches from the south of Norway. In the next 12 h, the system moved northward, the wind direction veered, and the H_s slowly decayed.

3.2. Climatology of Synoptic Evolutions Yielding Extreme Waves

The synoptic forcing of extreme wave heights at Forties at the time of maximum wave height is shown for the largest 18 events in the data set in Figure 6. Three of the four largest events (Figures 6a, 6c, and 6d) look very similar in terms of MSLP and wind fields: an extratropical cyclone is located over southern Scandinavia and an anticyclone to the west of the British Isles. This synoptic pattern also exists in events 6–12 and 14 (Figures 6f–6l and 6n). Events 2 (Figure 6d), 5 (Figure 6e), 13 (Figure 6m) and 15 (Figure 6o), 16 (Figure 6p), and 18 (Figure 6r) look distinctly different from the events discussed above. The large H_s values of these events are associated with south-easterly winds of an extratropical cyclone centered to the west of the British Isles. Event 17 (Figure 6n) is a northerly-event with the wind speed only large in the central North Sea region. Within the 100 largest H_s events, 53 were caused by northerly-winds (CCB events) and 47 events were caused by southerly-winds (WCB events). The clusters have different dynamical properties which ultimately relate to different wave heights at the Forties platform, with CCB events preferentially associated with the largest H_s events (Figure 3).

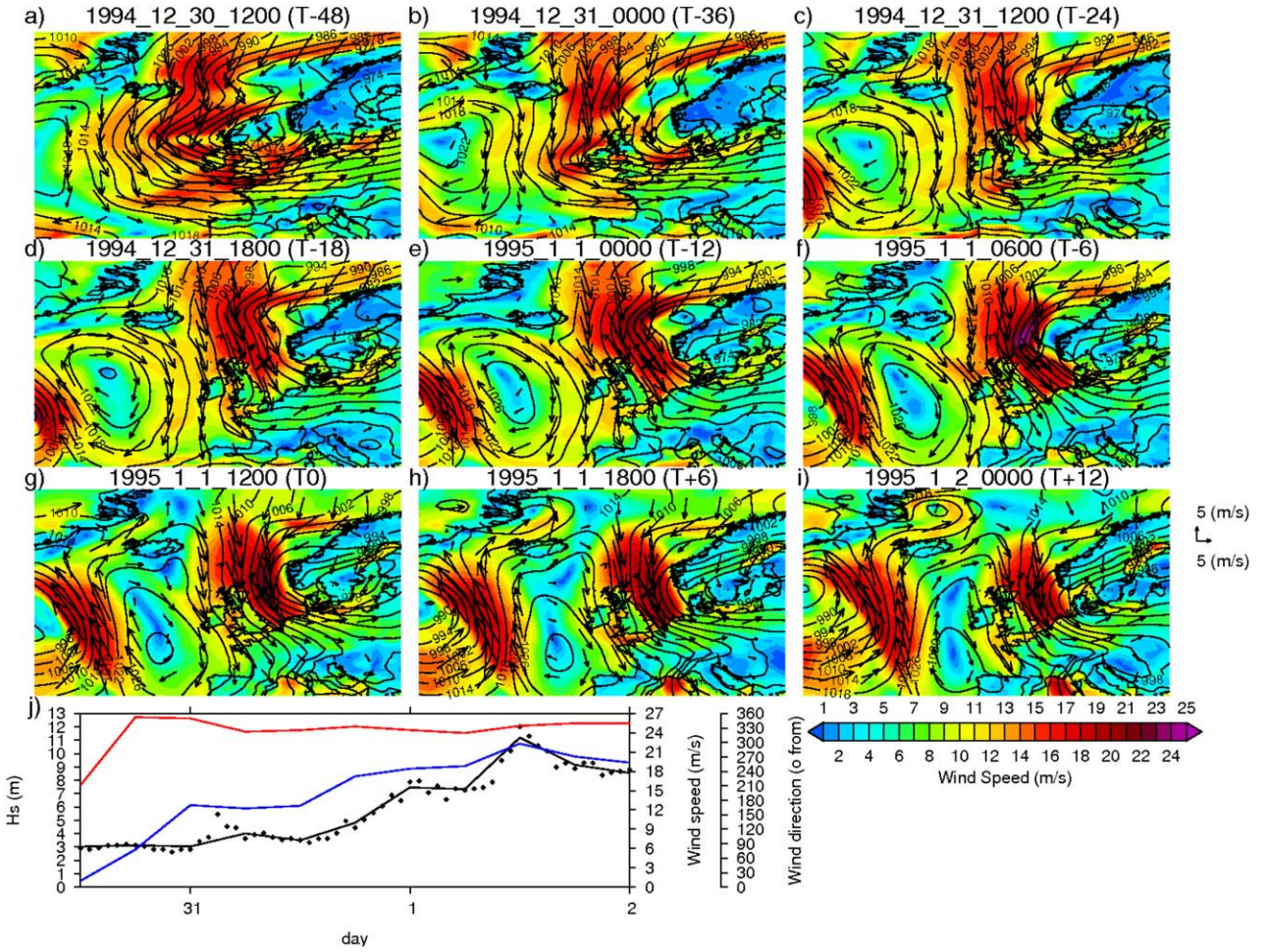

Figure 4. Synoptic evolution of the largest H_s at Forties on 1 January 1995. The colors represent 10 m wind speed (m s^{-1}), contours are MSLP (hPa), and the arrows show wind direction. The black cross denotes the location of the Forties platform: (a) T-48 h, (b) T-36 h, (c) T-24 h, (d) T-18 h, (e) T-12 h, (f) T-6 h, (g) T0, (h) T+6 h, and (i) T+12 h. The domain is 40°W–25°E, 40°N–75°N. (j) Time series at the Forties platform from T-48 to T+12 of measured H_s (black solid line is the 3 hourly average plotted at every 6 h and black dots are the raw data), wind speed (blue), and wind direction (red, ° from North) derived from ERA-I.

Figures 7a–7c shows the 1979–2015 climatology of MSLP, 10 m winds and 200 hPa winds (the latter chosen because 200 hPa is approximately the height of the jet stream). Figures 7d–7i show composite anomalies of the two types of directional wind events. For the CCB events, an anomalous low pressure is situated over southern Scandinavia (700 km to the east of the platform) and a high pressure anomaly is to the west of the British Isles (Figure 7d). The surface wind pattern (Figure 7e) highlights the surface cyclonic circulation over southern Scandinavia and associated strong northerly-winds in the CCB region in the North Sea. The 200 hPa wind speed (Figure 7f) shows the jet stream has a north-west to south-east tilt and the Forties platform is located on the jet's northern flank. By contrast, the southerly-wind events are dominated by a large anomalous low pressure region north-west of the Forties platform (Figure 7g). The anomalous surface winds have their maximum in the WCB region of the anomalous cyclone (Figure 7h). The associated 200 hPa wind speed is more zonal (than for the CCB events) and the Forties platform is located in the left jet exit region (Figure 7i), a region associated with intense wind storms [*Clark et al.*, 2009].

Composite analyses showing the evolution of synoptic forcing of extreme wave height events associated with northerly-and southerly-wind at the Forties platform are presented in Figures 8a–8i and 9a–9i, respectively, from 2 days before to 12 h after the time of the extreme wave height event. Two days before the northerly-wind events (T-48; Figure 8a), there is a pressure gradient between a high pressure system to the north east of the Azores and a low pressure system to the North of Scandinavia with associated near-westerly geostrophic winds. The low pressure system then deepens and moves slowly to the south. As

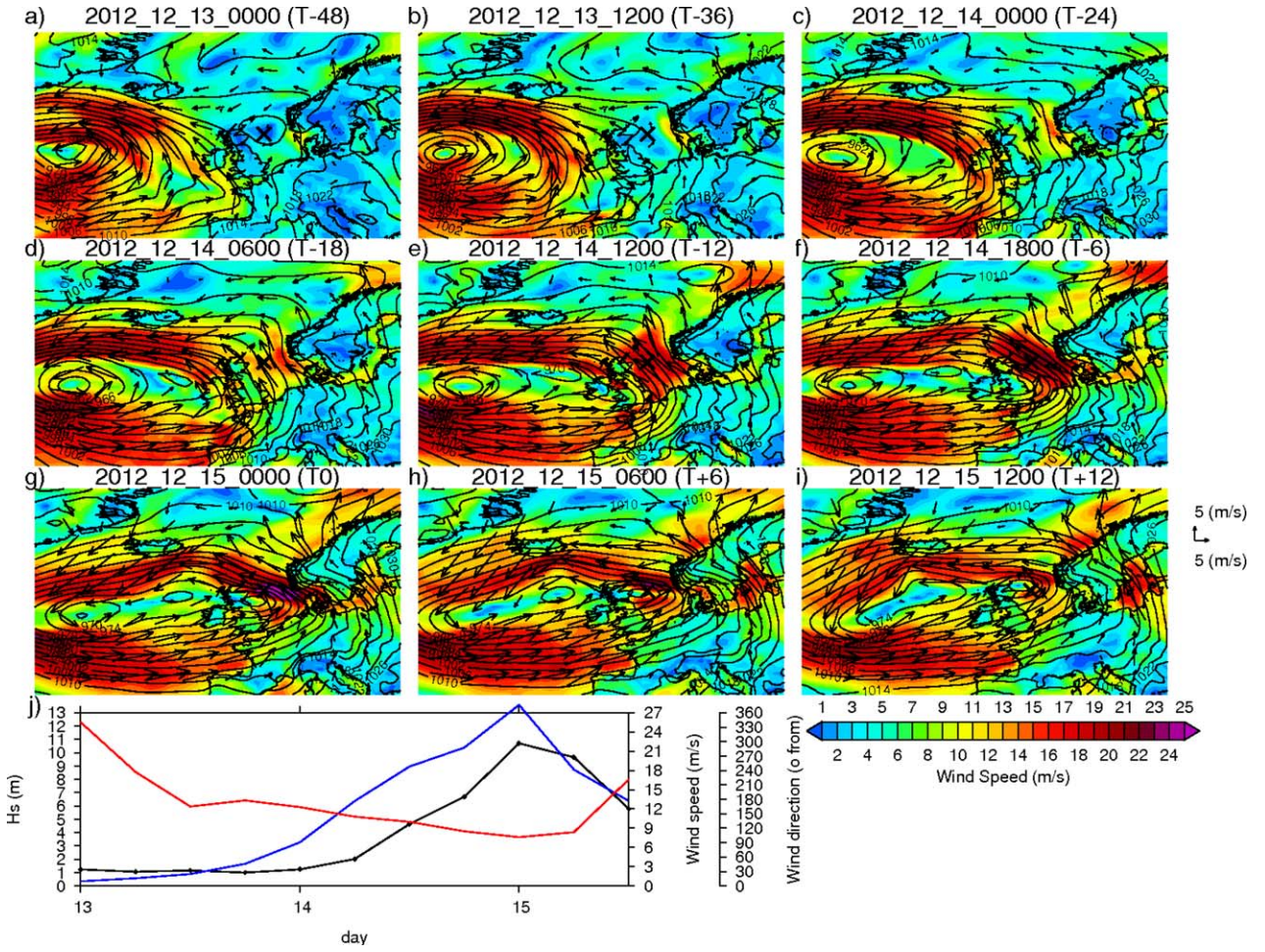

Figure 5. As for figure 4, but for synoptic evolution of the largest southerly H_s event (second largest H_s) at Forties on 15 December 2012.

shown in the time series (Figure 8j), the wind speed increases rapidly between 18 and 6 h before the event. This is a result of the strengthening of the north-east to south-west pressure gradient at the Forties platform. The directionality of the pressure gradient is important as it influences the size of the fetch available to the central North Sea. After the extreme wave height event, the H_s decays as the low pressure system moves to the east.

For the southerly-wind events, the composite cyclone is larger in size, but only the winds in the North Sea influence the waves (Figure 9). Compared to CCB events, the time evolutions of wind speed and H_s are more rapid with wind speed only starting to increase at T-24 and H_s at T-12 (compare Figures 8j and 9j). As the composite cyclone moves east and matures, the winds in the WCB region over the North Sea strengthen. The most rapid intensification of wind speed occurs between T-12 and T-6. At the time of maximum H_s (T0), the wind speed is strongest in the North Sea, although the Forties platform is not located in the area of maximum wind speed (unlike in Figure 8g for the northerly-wind events); instead the maximum wind speed is located approximately 50 km to the north east of the platform.

3.3. Extratropical Cyclone Tracks

The tracks of the cyclones associated with the extreme wave events at the Forties platform are shown in Figure 10. The locations of the cyclones at the time of their associated extreme wave event (indicated by the green squares) are clustered to the east and over (and to the north of) the British Isles for northerly and southerly-wind events, respectively. The locations of these clusters are thus consistent with the composite MSLP fields shown in Figures 8g and 9g for the northerly and southerly-wind events, respectively. For the northerly-wind events, the cyclone locations at the extreme wave event time have their greatest spread in

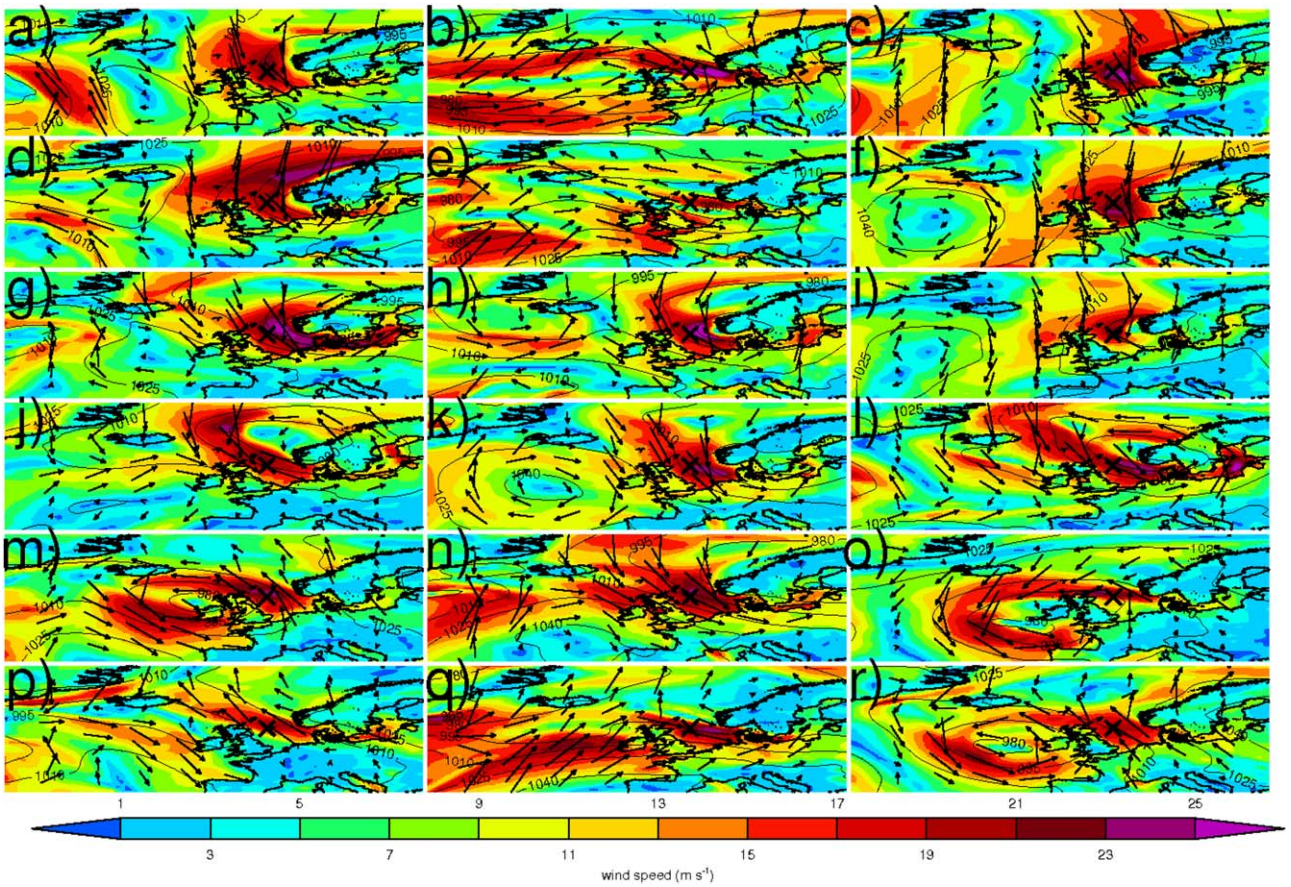

Figure 6. Synoptic situation at the time of maximum wave height for the 18 largest wave events at the Forties platform. The colors represent 10 m wind speed (m s^{-1}), contours are MSLP (hPa) and the arrows show the wind speed and direction. The black cross denotes the location of the Forties platform. Events decrease in maximum wave height from (a) to (r).

the zonal direction whereas for the southerly-wind events, the spread is more meridional. The tracks associated with the northerly-wind events tend to curve northward, generally reaching higher latitudes than the tracks associated with the southerly-wind events east of 30°W. This track curvature is consistent with the deflection of cyclones around the anticyclone to the west of the British Isles shown in the composite MSLP anomaly fields at the extreme event times in Figure 7d and in the evolution of the composite MSLP field in Figures 8a–8i. Cyclones associated with the northerly-wind events are also more likely to have their genesis region (inferred from the first tracked points which are indicated by red circles) north of 50°N. In contrast, the tracks associated with the southerly-wind events are typically relatively straight from the genesis region of the cyclones in the south western North Atlantic, consistent with the absence of an anticyclone for these events (Figures 7g and 9a–9i).

3.4. Sensitivity of Extreme Wave Height Events to the Precursor Environment

The sensitivities of the height of the extreme waves at the Forties platform to the precursor MSLP and U_{10} fields are shown in Figures 11–14 and separately for northerly and southerly-wind events. The sensitivity value at a given spatial point and time can be interpreted as the increase in wave height at the Forties platform at the event time (T0) associated with a one standard deviation increase in the value of the field (MSLP or U_{10}) at the given point and time; negative sensitivity values imply that decreases in the field are associated with an increase in wave height. Consequently, sensitivity values tend to have largest peak magnitudes at times closest to the event time. The interpretations of the sensitivity maps at the event time (T0) are first described here (plot g in Figures 11–14), followed by extension to the earlier and later times.

The sensitivity map of the wave height to MSLP for northerly-wind events at the event time (Figure 11g) has a dipole structure with low sensitivity over Denmark and high sensitivity over Iceland. Figure 11g implies that the largest wave heights are associated with the south-east to north-west pressure gradient

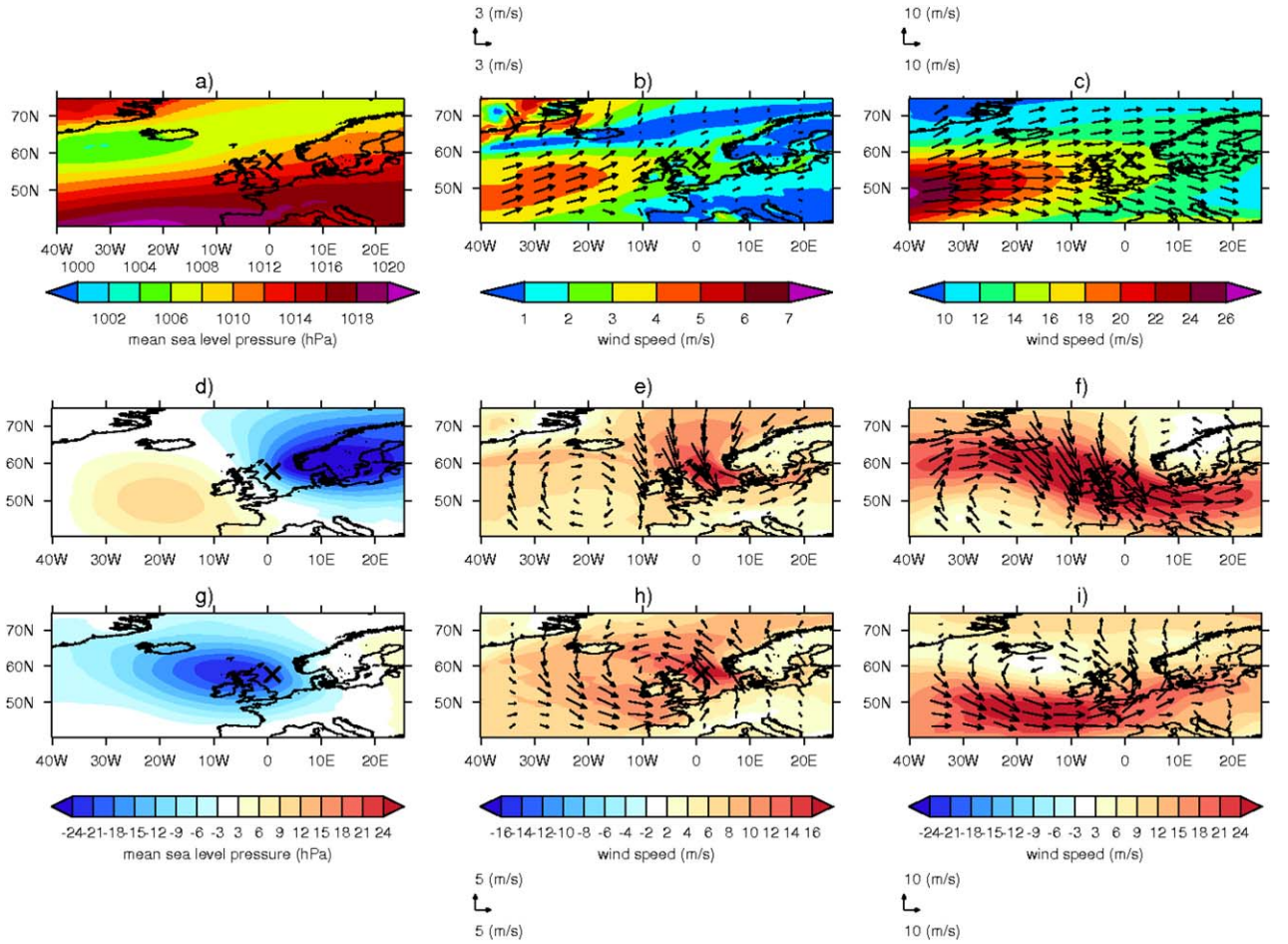

Figure 7. (a–c) 1979–2015 climatology of (a) MSLP, (b) 10 m wind speed and direction and (c) 200 hPa wind speed and direction. (d–i) Anomalies of the same fields (compared to climatology) for the top 100 extreme wave events at the Forties platform separated into (d–f) northerly and (g–i) southerly-wind events. The color bars for Figures 7g, 7h, and 7i also apply to Figures 7d, 7e and 7f, respectively. The black cross denotes the location of the Forties platform.

across the Forties platform at the time of the events; this is consistent with the simultaneous anomalously strong U_{10} (Figure 7e) due to the linear relationship between pressure gradient and geostrophic wind. Stronger U_{10} values in the vicinity of the Forties platform at the time of the events are associated with higher waves (Figure 12g).

In contrast, the sensitivity of the wave height to MSLP for southerly-wind events at the event time (Figure 13g) has a very different pattern to northerly-wind events. The sensitivities are weaker and regions of high-pressure have less of an impact. The dominant feature in Figure 13g is a region of negative sensitivity to the south of the platform. This implies that it is the depth of the anomalous low in the southern North Sea that is directly associated with the wave height in these events. The sensitivity map for U_{10} at the event time (Figure 14g) shows a band of positive sensitivity to the east of platform. The Forties platform lies in a region of near zero sensitivity to U_{10}. This map suggests that, in contrast to the equivalent map for the northerly-wind events, the wave heights of southerly-wind events are not directly associated with the strength of the winds at the platform, but instead are associated with the strength of the winds to the east; this suggests that the relevant fetch for southerly-wind events at the Forties platform extends east to the strait between Norway and Denmark.

There is a consistent evolution in the patterns of sensitivity from T-48 to T+12 in each of the sensitivity figures (Figures 11–14). For the northerly-wind events, the dipole pattern of MSLP sensitivity present at T0 rotates and strengthens from a zonal dipole visible at T-18 (prior to this, from T-48 to T-24, only the precursor positive pole is present; Figure 11). The region of positive sensitivity to U_{10} associated with the MSLP sensitivity dipole moves southeastward from its location directly to the south and east of Iceland at T-24 to

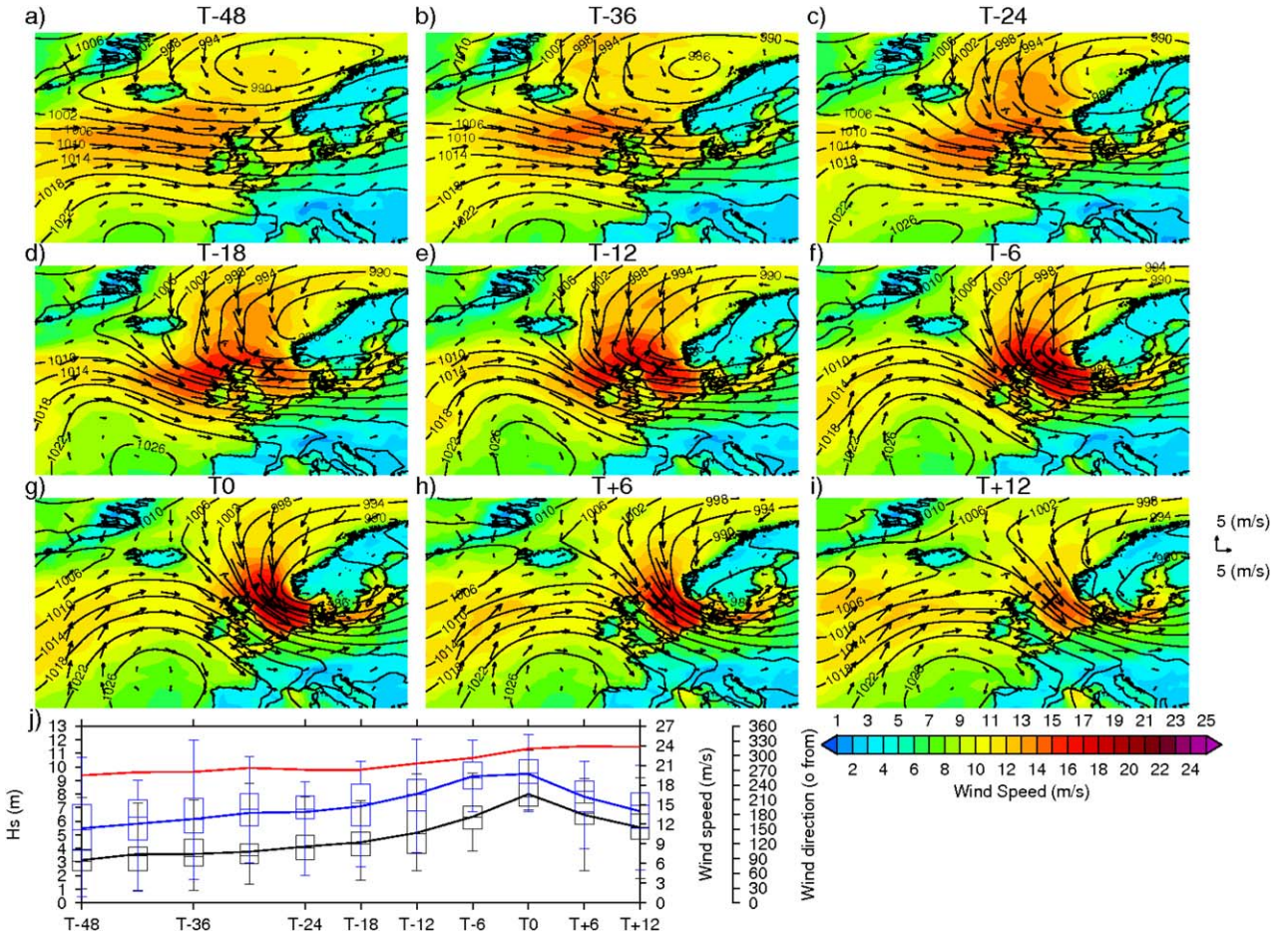

Figure 8. As for Figure 4, but for composite of the synoptic evolution of the largest wave events at the Forties platform with northerly winds. The boxes in Figure 8j show the median and the upper and lower quartiles of the data; the whiskers show the minimum and maximum values.

form a band colocated with the North Sea from T-12 to T+12 (Figure 12); the evolution of this positive sensitivity region is consistent with the paradigm that extreme wave events are influenced by strong winds some distance upstream at earlier times due to the dependence of extreme wave heights on fetch. Additionally, a large and strongly negative region of MSLP sensitivity is present in the southeast of the domain at T-48 that moves eastward and/or decays with time. While it is plausible that this region downstream of the Forties platform could influence the development of the synoptic weather systems upstream, it is more likely that this negative sensitivity region is simply a consequence of the typical large-scale pattern of synoptic-scale developments i.e., strong cyclones typically occur once every few days. The interpretation made of this negative sensitivity region present at T-48 is an example of the caveat explained in section 2.5: the sensitivities plotted are merely associations and their interpretation is dependent on dynamical plausibility.

For the southerly-wind events, the region of negative sensitivity to MSLP found to the south of the platform at the event time has developed by gradually moving eastward from a strong region of negative sensitivity to the west of the British Isles shown at T-36 (Figure 13g). A band of positive sensitivity to U_{10} that lies to the east of the platform from T-24 to T0 is associated with the source of waves which affect Forties. The strongest sensitivity in this region is at T-6 (Figure 14f).

4. Discussion and Conclusions

The largest extreme H_s events at an offshore platform in the central North Sea are found to be associated with northerly-winds within extratropical cyclones which reach their maximum intensity, on average,

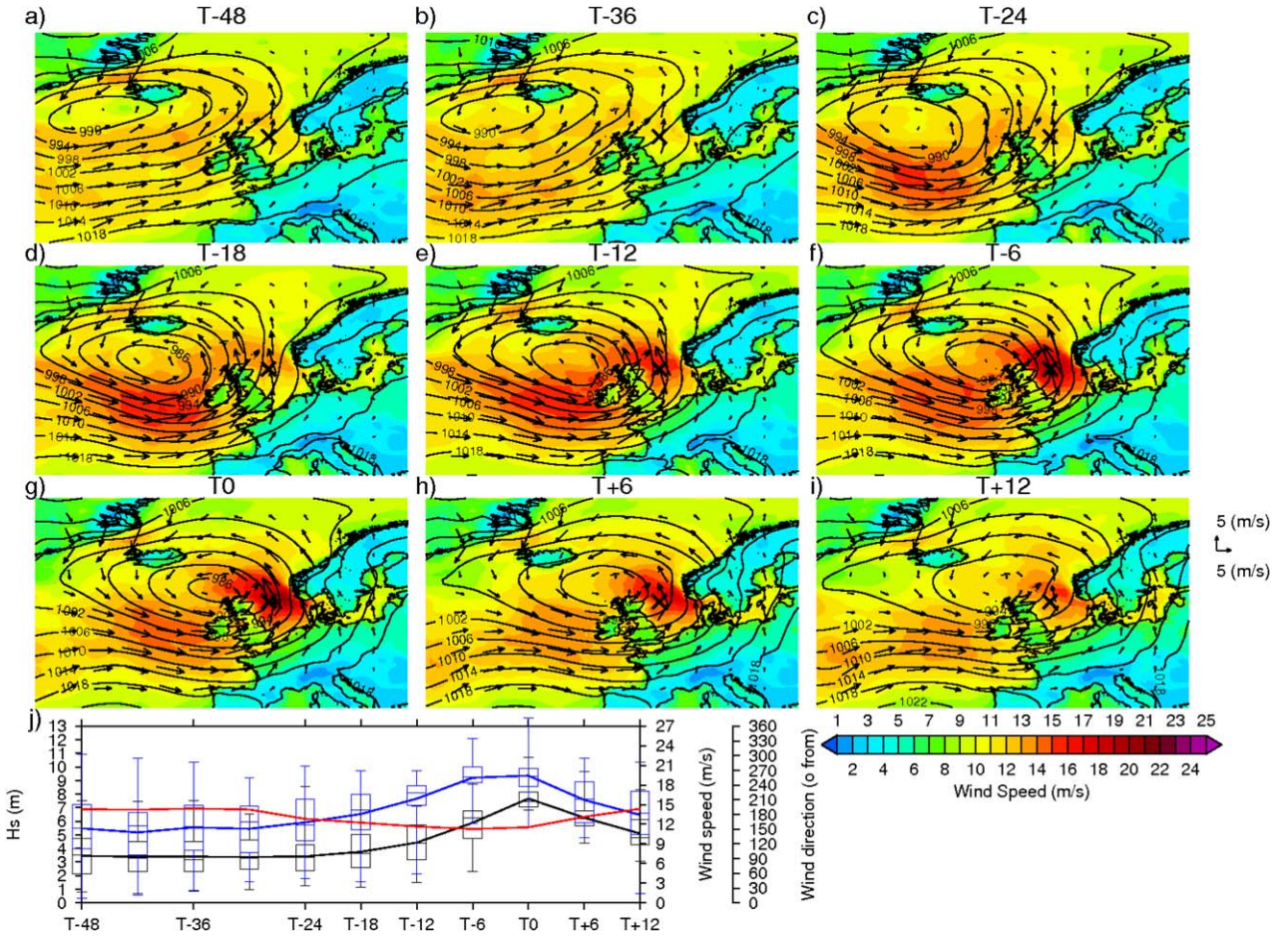

Figure 9. As for Figure 8, but for composite of the synoptic evolution of the largest wave events at the Forties platform with southerly winds.

700 km to the east of the platform. This situation, combined with a blocking high pressure to the west of the British Isles, drives winds along the longest fetch available to the North Sea. These northerly-winds are usually associated with the CCB of the cyclone. This association has been recognized previously for individual case studies. For example, the strong winds in the CCB of extratropical cyclone Quirin (14 February 2011)

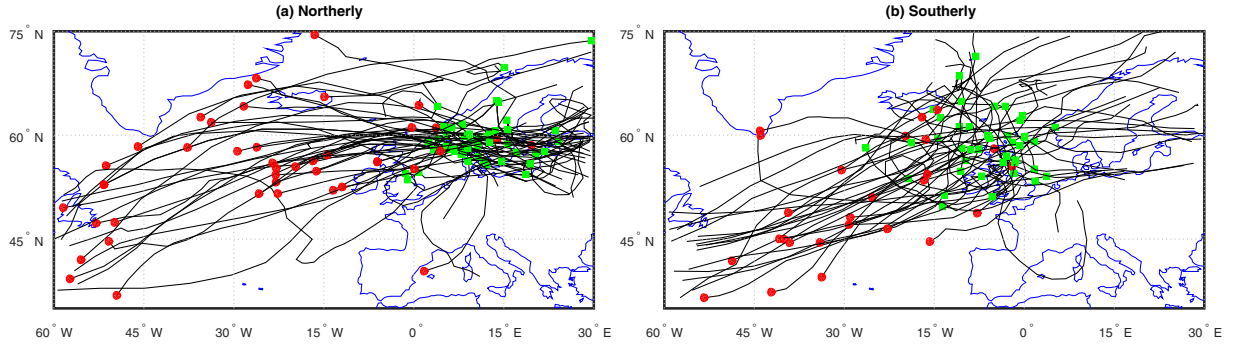

Figure 10. Tracks of extratropical cyclones associated with the largest wave events at Forties for (a) northerly and (b) southerly-wind events. The red circle marks the start point of each track (some tracks begin outside the domain shown) and the green square is time of the associated extreme wave event. Tracks for 52 of the 53 of the northerly-wind events and 42 of the 47 southerly-wind events are plotted. Two of the missing tracks are for events occurring on the last day of a season, likely resulting from the track diagnosis being performed separately for the different seasons. For two events, the tracking algorithm has not identified the low pressure center associated with the strong winds at the Forties platform and for the remaining two events the strong winds exist on the east flank of an anticyclone.

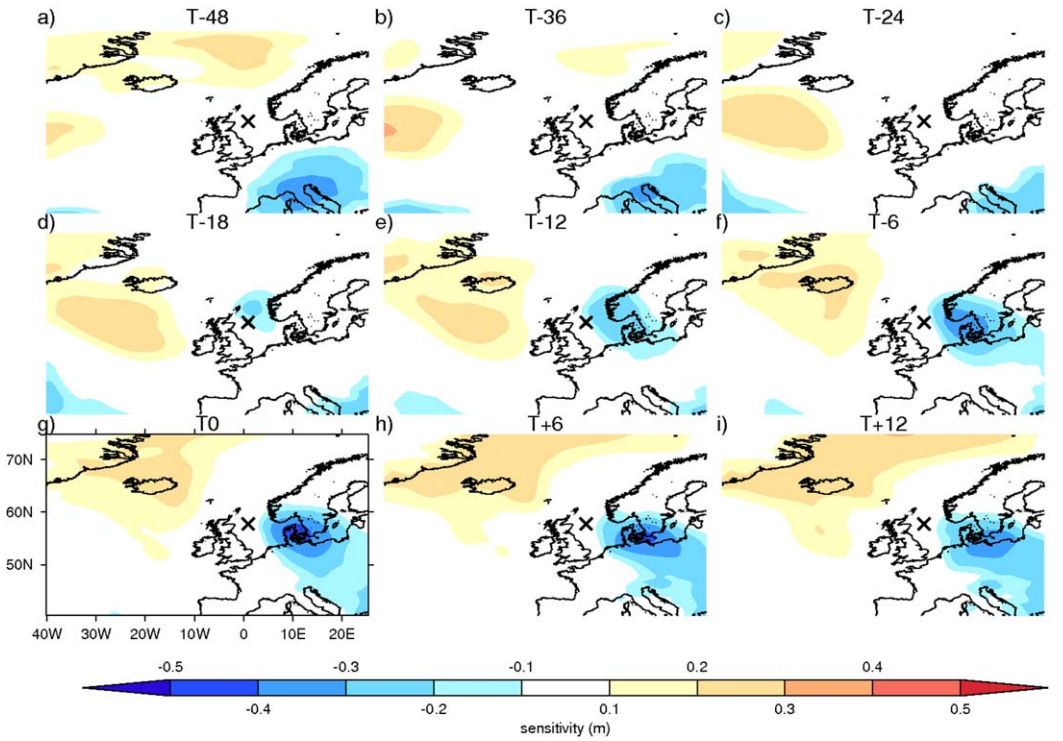

Figure 11. Sensitivity of H_s to MSLP at the Forties platform for northerly-wind events: (a) T-48 h, (b) T-36 h, (c) T-24 h, (d) T-18 h, (e) T-12 h, (f) T-6 h, (g) T0, (h) T+6 h, and (i) T+12 h. The time of the extreme wave event is highlighted by the black border.

were responsible for the largest H_s ever observed in the North Atlantic using satellites [*Hanafin et al.*, 2012]. *Ponce de León and Guedes Soares* [2014] also noted that freak waves are more likely to occur in the CCB region of extratropical cyclones in the open ocean.

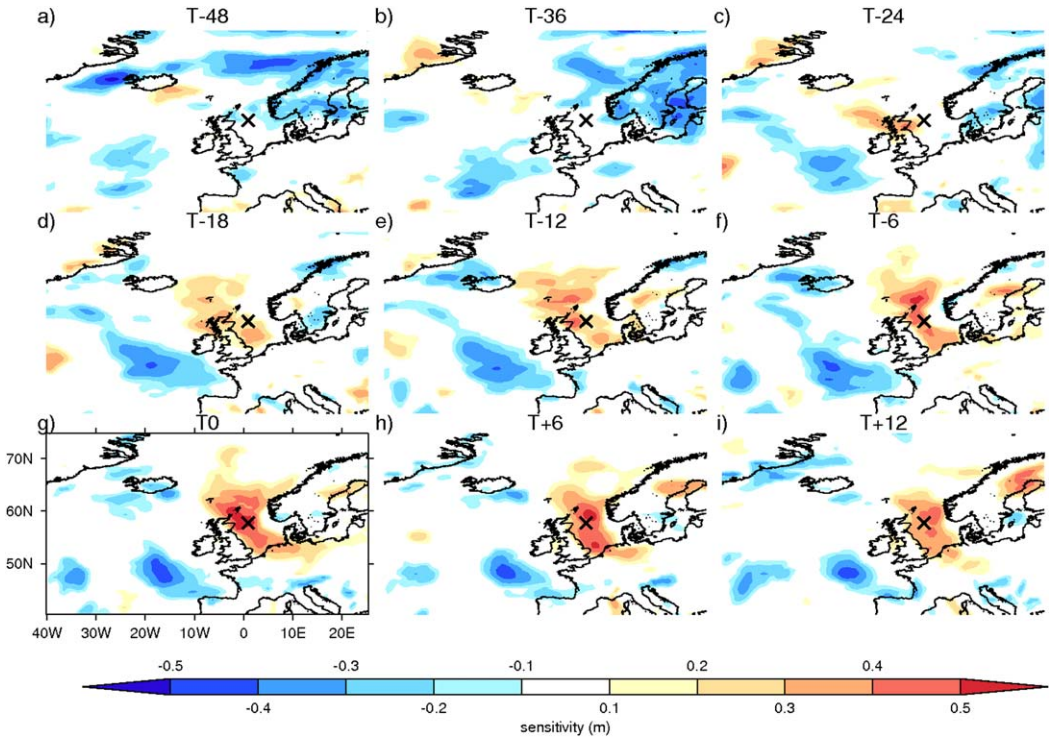

Figure 12. As for Figure 11, but for sensitivity to U_{10} for northerly-wind events.

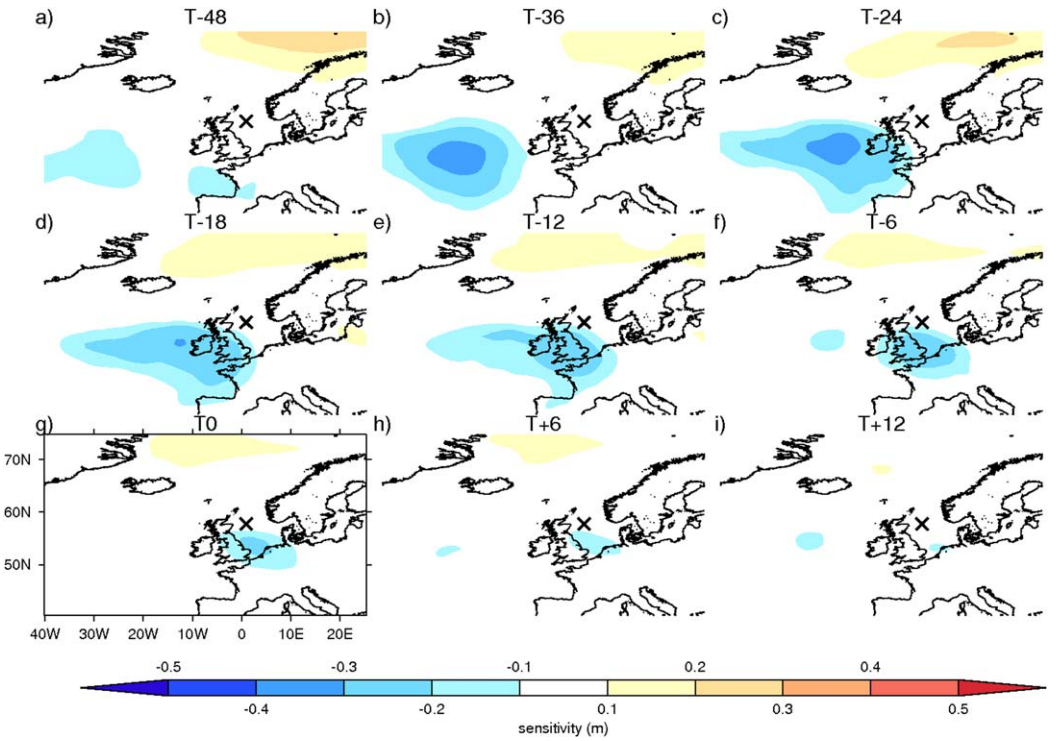

Figure 13. As for Figure 11, but for sensitivity to MSLP for southerly-wind events.

While the largest H_s events are shown to be associated with CCB events, nearly half (47%) of the top 100 events occur in southerly-winds within the WCB of cyclones. The associated cyclones tend to take a more southerly track (compared to the CCB events) and are also associated with strong wind speeds. The

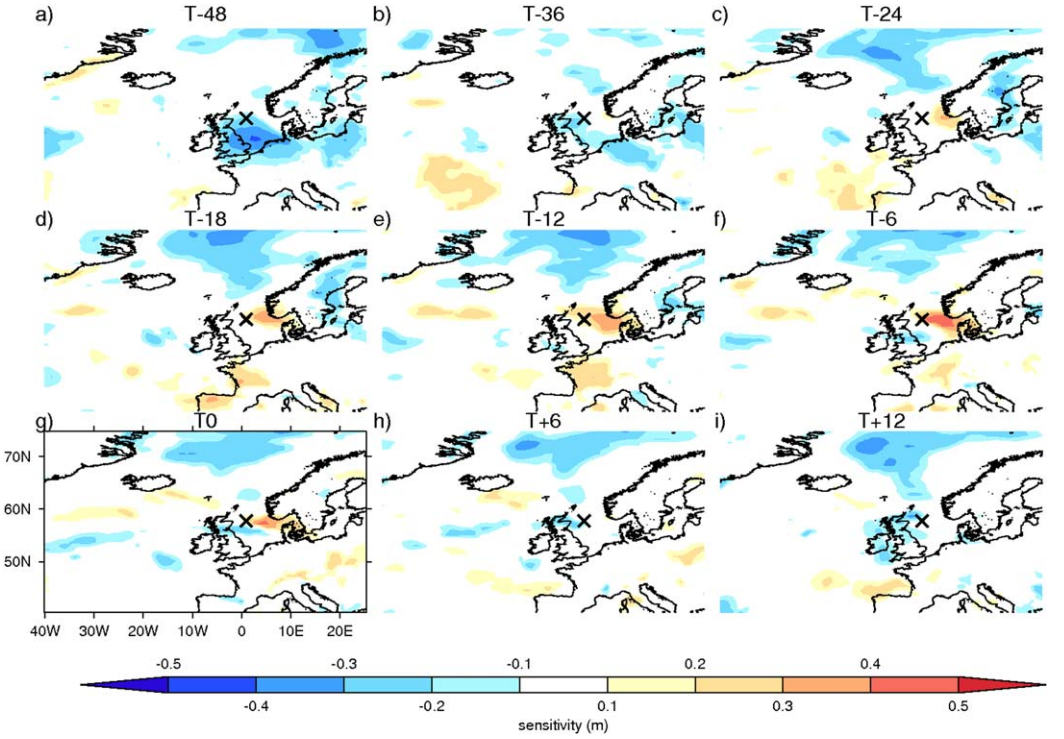

Figure 14. As for Figure 11, but for sensitivity to U_{10} for southerly-wind events.

extratropical cyclones yielding the southerly-wind events intensify in the left jet exit region. Extratropical cyclones here are known to be intense due to deceleration out of the jet stream which results in upper level divergence and upward motion [*Clark et al*., 2009]. It is plausible that events from the south can lead to freak wave conditions due to the large wave height and short wave period from the limited fetch. This creates a steep sea state which is more favorable for freak wave occurrence, as was observed in December 2012 [*Gibson et al*., 2014].

The ensemble sensitivity technique provides information on the likely predictability horizon of extreme wave events. For example, the MSLP sensitivity for the northerly-wind events is visible at T-18. In contrast, southerly-wind extreme wave events may be harder to forecast as the sensitivity (especially wind speed) is not as prominent as for northerly-wind events at longer lead times, although there is a relationship between MSLP to the west of the British Isles at T-36 to large wave heights at the Forties platform. This information could be included with known inadequacies of the forecast model to allow the forecaster to provide an improved warning of possible extreme wave events. This would have to be studied in detail using a large set of forecast data which is outside the scope of this paper.

The conclusions of this paper are as follows:

1. The largest wave events occur in the central North Sea when a low pressure system is situated over southern Scandinavia. This gives rise to a long northerly fetch associated with strong winds in the CCB of the associated extratropical cyclone. This atmospheric situation occurs when there is a north-west to south-east tilt in the jet stream over the British Isles.
2. Southerly-wind events can also create large wave heights despite the limited fetch. Southerly-wind events are associated with a zonal jet and extratropical cyclones that intensify rapidly in the jet left exit region of the jet stream.
3. The northerly-wind extreme H_s events demonstrate sensitivity to an anticyclone (high pressure system) forming west/northwest of the British Isles from at least 48 h before the extreme wave event and a cyclone forming to the east of the British Isles from 18 h before the event. Southerly-wind extreme events demonstrate sensitivity to a cyclone that crosses from the west to east of the British Isles from 36 h before the extreme H_s event.

Acknowledgments

This research was supported by Innovate UK and BP Operating Company Limited (project number 508949). We thank BP for allowing us to use their platform data and PhysE Ltd for providing us with meta-data. We are grateful to Kevin Hodges for providing the extratropical cyclone tracks. Caroline Macé undertook an important preliminary study of the wave data available. ERA-Interim data can be obtained from http://apps.ecmwf.int/datasets/data/interim-full-daily/levtype=sfc/. The first two ocean wave data time series were provided by BP Operating Company Limited, for further details contact coauthor Oliver Jones. The third ocean wave time series was provided by Jean-Raymond Bidlot (jean.bidlot@ecmwf.int). We thank two anonymous reviewers for their help in improving this manuscript.

References

Baker, L. H., S. L. Gray, and P. A. Clark (2014), Idealised simulations of sting-jet cyclones, *Q. J. R. Meteorol. Soc.*, *140*, 96–110.

Bidlot, J.-R., D. J. Holmes, P. A. Wittmann, R. Lalbeharry, and H. S. Chen (2002), Intercomparison of the performance of operational ocean wave forecasting systems with buoy data, *Weather Forecast.*, *17*(2), 287–310.

Breivik, Ø., O. J. Aarnes, S. Abdalla, J.-R. Bidlot, and P. A. Janssen (2014), Wind and wave extremes over the world oceans from very large ensembles, *Geophys. Res. Lett.*, *41*, 5122–5131, doi:10.1002/2014GL060997.

Browning, K. A. (2005), Observational synthesis of mesoscale structures within an explosively developing cyclone, *Q. J. R. Meteorol. Soc.*, *131*(606), 603–623.

Browning, K. A., and Roberts, N. M. (1994), Structure of a frontal cyclone, *Q. J. R. Meteorol. Soc.*, *120*(520), 1535–1557.

Camus, P., F. J. Méndez, I. J. Losada, M. Menéndez, A. Espejo, J. Pérez, A. Rueda, and Y. Guanche (2014), A method for finding the optimal predictor indices for local wave climate conditions, *Ocean Dyn.*, *64*(7), 1025–1038.

Cardone, V. J., B. T. Callahan, H. Chen, A. T. Cox, M. A. Morrone, and V. R. Swail (2015), Global distribution and risk to shipping of very extreme sea states (VESS), *Int. J. Climatol.*, *35*(1), 69–84.

Cavaleri, L., F. Barbariol, A. Benetazzo, L. Bertotti, J.-R. Bidlot, P. A. Janssen, and N. Wedi (2016), The Draupner wave: A fresh look and the emerging view, *J. Geophys. Res. Oceans*, *121*, 6061–6075, doi:10.1002/2016JC011649.

Clark, A. J., C. J. Schaffer, W. A. Gallus, and K. Johnson-OMara (2009), Climatology of storm reports relative to upper-level jet streaks, *Weather Forecast.*, *24*(4), 1032–1051.

Dacre, H. F., and S. L. Gray (2009), The spatial distribution and evolution characteristics of North Atlantic cyclones, *Mon. Weather Rev.*, *137*, 99–115.

Dacre, H. F., and S. L. Gray (2013), Quantifying the climatological relationship between extratropical cyclone intensity and atmospheric precursors, *Geophys. Res. Lett.*, *40*, 2322–2327, doi:10.1002/grl.50105.

Dee, D. P., et al. (2011), The ERA-Interim reanalysis: Configuration and performance of the data assimilation system, *Q. J. R. Meteorol. Soc.*, *137*(656), 553–597.

Feser, F., M. Barcikowska, O. Krueger, F. Schenk, R. Weisse, and L. Xia (2015), Storminess over the North Atlantic and northwestern Europe: A review, *Q. J. R. Meteorol. Soc.*, *141*(687), 350–382.

Garcies, L., and V. Homar (2009), Ensemble sensitivities of the real atmosphere: Application to Mediterranean intense cyclones, *Tellus A*, *61*(3), 394–406.

Gemmrich, J., J. Thomson. W. E. Rogers, A. Pleskachevsky, and S. Lehner (2016), Spatial characteristics of ocean surface waves, *Ocean Dyn.*, *66*(8), 1025–1035.

Gibson, R., M. Christou, and G. Feld (2014), The statistics of wave height and crest elevation during the December 2012 storm in the North Sea, *Ocean Dyn.*, *64*(9), 1305–1317.

Hanafin, J. A., et al. (2012), Phenomenal Sea states and swell from a North Atlantic storm in February 2011: A Comprehensive analysis, *Bull. Am. Meteorol. Soc.*, *93*(12), 1825–1832.

Hewson, T. D., and U. Neu (2015), Cyclones, windstorms and the IMILAST project, *Tellus A*, *67*, 27128.
Hodges, K. I. (1994), A general method for tracking analysis and its application to meteorological data, *Mon. Weather Rev.*, *122*, 2573–2586.
Hodges, K. I., R. W. Lee, and L. Bengtsson (2011), A comparison of extratropical cyclones in recent reanalyses ERA-Interim, NASA MERRA, NCEP CFSR, and JRA-25, *J. Clim.*, *24*(18), 4888–4906.
Hoskins, B. J., and K. I. Hodges (2002), New perspectives on the northern hemisphere winter storm tracks, *J. Atmos. Sci.*, *59*, 1041–1061.
Kudryavtsev, V., P. Golubkin, and B. Chapron (2015), A simplified wave enhancement criterion for moving extreme events, *J. Geophys. Res. Oceans*, *120*, 7538–7558, doi:10.1002/2015JC011284.
Leadbetter, M. R. (1991), On a basis for "Peaks over Threshold" modeling, *Stat. Probab. Lett.*, *4*(11), 357–362.
Martínez-Alvarado, O., S. L. Gray, J. L. Catto, and P. A. Clark (2012), Sting jets in intense winter North-Atlantic windstorms, *Environ. Res. Lett.*, *7*, 24014.
Martínez-Alvarado, O., L. H. Baker, S. L. Gray, J. Methven, and R. S. Plant (2014), Distinguishing the Cold Conveyor Belt and Sting Jet Airstreams in an Intense Extratropical Cyclone, *Mon. Weather Rev.*, *142*, 2571–2595.
Odell, L., P. Knippertz, S. Pickering, B. Parkes, and A. Roberts (2013), The Braer storm revisited, *Weather*, *68*(4), 105–111.
Ortiz-Royero, J. C., L. J. Otero, J. C. Restrepo, J. Ruiz, and M. Cadena (2013), Cold fronts in the Colombian Caribbean Sea and their relationship to extreme wave events, *Nat. Hazards Earth Syst. Sci.*, *13*(11), 2797–2804.
Pingree-Shippee, K. A., N. J. Shippee, and D. E. Atkinson (2016), Overview of Bering and Chukchi sea wave states for four severe storms following common synoptic tracks, *J. Atmos. Oceanic Technol.*, *33*(2), 283–302.
Pinto, J. G., I. Gómara, G. Masato, H. F. Dacre, T. Woollings, and R. Caballero (2014), Large-scale dynamics associated with clustering of extratropical cyclones affecting Western Europe, *J. Geophys. Res. Atmos.*, *119*, 13,704–13,719, doi:10.1002/2014JD022305.
Ponce de León, S., and C. Guedes Soares (2014), Extreme wave parameters under North Atlantic extratropical cyclones, *Ocean Modell.*, *81*, 78–88.
Reistad, M., A. Magnusson, S. Haver, O. Gudmestad, and D. Kvamme (2005), How severe wave conditions are possible on the Norwegian Continental Shelf?, *Mar. Struct.*, *18*(5-6), 428–450.